The impact of MEG source reconstruction method on source-space connectivity estimation: A comparison between minimum-norm solution and beamforming

Ana-Sofía Hincapié, Jan Kujala, Jérémie Mattout, Annalisa Pascarella, Sebastien Daligault, Claude Delpuech, Domingo Mery, Diego Cosmelli, Karim Jerbi

PII: S1053-8119(17)30331-2
DOI: http://dx.doi.org/10.1016/j.neuroimage.2017.04.038
Reference: YNIMG13979

To appear in: *NeuroImage*

Received date: 19 August 2016
Revised date: 1 April 2017
Accepted date: 15 April 2017

Cite this article as: Ana-Sofía Hincapié, Jan Kujala, Jérémie Mattout, Annalisa Pascarella, Sebastien Daligault, Claude Delpuech, Domingo Mery, Diego Cosmelli and Karim Jerbi, The impact of MEG source reconstruction method on source-space connectivity estimation: A comparison between minimum-norm solution and beamforming, *NeuroImage* http://dx.doi.org/10.1016/j.neuroimage.2017.04.038

The impact of MEG source reconstruction method on source-space connectivity estimation: A comparison between minimum-norm solution and beamforming

Ana-Sofía Hincapié[a,b,c,d*1,2,3,4], Jan Kujala[b,e2,5], Jérémie Mattout[b2], Annalisa Pascarella[f6], Sebastien Daligault[g7], Claude Delpuech[b,g2,7], Domingo Mery[c3], Diego Cosmelli[d4], Karim Jerbi[a,b1,2]

[a]Psychology Department, University of Montreal, Quebec, Canada.

[b]Lyon Neuroscience Research Center, DyCog team, Inserm U1028, CNRS UMR5292, Lyon, France.

[c]Department of Computer Science, Pontificia Universidad Católica de Chile, Santiago de Chile, Chile.

[d]Escuela de Psicología, Pontificia Universidad Católica de Chile and Interdisciplinary Center for Neurosciences, Pontificia Universidad Católica de Chile, Santiago de Chile, Chile

[e]Department of Neuroscience and Biomedical Engineering, Aalto University, Espoo, Finland.

[f]Consiglio Nazionale delle Ricerche (CNR - National Research Council), Rome, Italy

[g]MEG Center, CERMEP, Lyon, France

ashincap@uc.cl

jan.kujala@aalto.fi

jeremie.mattout@inserm.fr

a.pascarella@iac.cnr.it

daligault@cermep.fr

claude.delpuech@inserm.fr

dmery@ing.puc.cl

dcosmelli@uc.cl

karim.jerbi@umontreal.ca

*Correspondence should be addressed to: Ana-Sofía Hincapié, Psychology Department, University of Montreal, Pavillon Marie-Victorin, 90, avenue Vincent d'Indy, Quebec, Canada.

[1] Postal address: Pavillon Marie-Victorin, 90, avenue Vincent d'Indy, Montreal, Québec, Canada.
[2] Postal address: INSERM U1028, 69675 Bron Cedex, France.
[3] Postal address: Av. Vicuña Mackenna 4860 (143), Macul, Santiago de Chile, Chile.
[4] Postal address: Av. Vicuña Mackenna 4860, Macul, Santiago de Chile, Chile.
[5] Postal address: P.O. Box 15100, FI-00076 Aalto, Finland.
[6] Postal address: Via dei Taurini, 19 - 00185 Roma, Italy.
[7] Postal address: INSERM U1028, 69675 Bron Cedex, France.

Abstract

Despite numerous important contributions, the investigation of brain connectivity with magnetoencephalography (MEG) still faces multiple challenges. One critical aspect of source-level connectivity, largely overlooked in the literature, is the putative effect of the choice of the inverse method on the subsequent cortico-cortical coupling analysis. We set out to investigate the impact of three inverse methods on source coherence detection using simulated MEG data. To this end, thousands of randomly located pairs of sources were created. Several parameters were manipulated, including inter- and intra-source correlation strength, source size and spatial configuration. The simulated pairs of sources were then used to generate sensor-level MEG measurements at varying signal-to-noise ratios (SNR). Next, the source level power and coherence maps were calculated using three methods (a) L2-Minimum-Norm Estimate (MNE), (b) Linearly Constrained Minimum Variance (LCMV) beamforming, and (c) Dynamic Imaging of Coherent Sources (DICS) beamforming. The performances of the methods were evaluated using Receiver Operating Characteristic (ROC) curves. The results indicate that beamformers perform better than MNE for coherence reconstructions if the interacting cortical sources consist of point-like sources. On the other hand, MNE provides better connectivity estimation than beamformers, if the interacting sources are simulated as extended cortical patches, where each patch consists of dipoles with identical time series (high intra-patch coherence). However, the performance of the beamformers for interacting patches improves substantially if each patch of active cortex is simulated with only partly coherent time series (partial intra-patch coherence). These results demonstrate that the choice of the inverse method impacts the results of MEG source-space coherence analysis, and that the optimal choice of the inverse solution depends on the spatial and synchronization profile of the interacting cortical sources. The insights revealed here can guide method selection and help improve data interpretation regarding MEG connectivity estimation.

Keywords

Brain connectivity, Magnetoencephalography (MEG), Minimum Norm Estimate (MNE), Linearly Constrained Minimum Variance (LCMV), Beamforming, Dynamic Imaging of Coherent Sources (DICS)

1. Introduction

Interactions between neural assemblies in different brain structures are a hallmark of healthy brain function (Mesulam 1990; Varela et al. 2001; Luo et al. 2010; Mišić & Sporns 2016). The ability to reliably measure the dynamics of cerebral networks is therefore of utmost importance when it comes to elucidating the neural basis of large-scale integration in health and monitoring its breakdown in disease (Schnitzler & Gross 2005; Lopes da Silva 2013; Pittau & Vulliemoz 2015). Given the diversity of available neuroimaging and brain recording

techniques, numerous functional brain connectivity measures have been used (e.g. Schoffelen & Gross 2009; Friston et al. 2013; Engel et al. 2013; O'Neill et al. 2015). One technique that is particularly well suited for the detection of large-scale interactions among neural assemblies is magnetoencephalography (MEG) (Hämäläinen et al. 1993; Dalal et al. 2009; Baillet et al. 2001; Gross et al. 2013; O'Neill et al. 2015). The millisecond-range temporal resolution of MEG allows us to probe the electrophysiological mechanisms that underlie functional brain connectivity (Schölvinck et al. 2013), and its role in sensory, motor and higher-order cognitive tasks (Lopes da Silva 2013; Jerbi et al. 2007; Gross et al. 2003; Schnitzler & Gross 2005; Meeren et al. 2013; Simanova et al. 2015) as well as in the resting-state (Cabral et al. 2014; de Pasquale et al. 2012; Hipp et al. 2012; Schölvinck et al. 2013; O'Neill et al. 2015; Henson et al. 2007; van Diessen et al. 2015; Garcés et al. 2016; Colclough et al. 2016).

Although sensor-level analyses of MEG recordings have provided important insights into brain function, the estimation of neuronal interactions at the source level is key to elucidating the role of large-scale brain networks in health and disease. To achieve this goal, one needs, first of all, to reconstruct the source time series that underlie the sensor-level measurements.

This is an ill-posed inverse problem since there is no unique solution (an infinite number of current density distributions result in zero magnetic field outside the head) and furthermore there is no continuous dependency of the solution from the data (i.e. small variations in source space can lead to large perturbations in data space). Given that the Maxwell equations are linear, it is impossible to choose between an infinite number of equally good solutions, without prior knowledge, additional constraints or both. Numerous methods have been proposed to tackle this inverse problem (Baillet et al. 2001; Küçükaltun-Yildirim et al. 2006; Gross et al. 2013). The specificity of each technique depends on the assumption that is made about the properties of the neural sources and on the way it incorporates various forms of a priori information, if any is available. One of the earliest and most widely used inverse methods is the Minimum Norm Estimate (MNE) (Dale & Sereno 1993; Hämäläinen & Ilmoniemi 1984; Hämäläinen & Ilmoniemi 1994; Sarvas 1987; Matsuura & Okabe 1995; Wang et al. 1993; Baillet et al. 2001; Hauk 2004; David et al. 2002; Attal & Schwartz 2013; Lin et al. 2006; Liu et al. 1998; Grave de Peralta Menendez et al. 1997; Hsiao et al. 2015; Cheng et al. 2015; Stenroos & Hauk 2013; Meeren et al. 2013; Palva et al. 2010; Mattout et al. 2005; Chang et al. 2015; Simanova et al. 2015; Kanamori et al. 2013). In principle, MNE searches for a

source distribution with the minimum (L2-norm) current that gives the best account of the measured data. Another popular family of MEG inverse methods is the beamformer approach (Van Veen et al. 1997; Gross et al. 2001; Hadjipapas et al. 2005; Küçükaltun-Yildirim et al. 2006; Barnes & Hillebrand 2003; Barnes et al. 2004; Ikezawa et al. 2011; Sekihara et al. 2001; Quraan et al. 2011; Hillebrand & Barnes 2005; Kujala et al. 2012; Kujala et al. 2008; Darvas et al. 2004; Popescu et al. 2008; Litvak et al. 2010; Laaksonen et al. 2012; Gross et al. 2003; Spaak et al. 2014; Rossiter et al. 2012; Muthuraman et al. 2015; Hui et al. 2010; Diwakar et al. 2011). Beamformers scan the source space through a set of spatial filters designed to pass the brain activity from a specified location while attenuating activity originating at other locations. Interestingly, although beamformers and MNE are among the most commonly used methods in MEG source level analysis (Sorrentino & Pascarella 2011; Hansen et al. 2010; Baillet et al. 2001), these techniques have primarily been compared in terms of source localization accuracy, but their effect on subsequent source-level connectivity reconstruction is only poorly understood and has been largely overlooked in the literature.

The differences between available methods are largely driven by the assumptions they make on the sources or on the character of the noise. While MNE assumes a Gaussian distribution for the noise, beamformers assume that the noise is uncorrelated with the sources. One theoretical difference regarding connectivity analysis is that beamformers assume the sources underlying the measurements to be uncorrelated (Van Veen et al. 1997) while MNE does not (Hämäläinen & Ilmoniemi 1984; Hämäläinen & Ilmoniemi 1994). Several studies have sought to assess the effect of method selection on source localization and power mapping (Liljeström et al. 2005; Darvas et al. 2004; Küçükaltun-Yildirim et al. 2006; Mattout et al. 2006; Sekihara et al. 2005; Hauk et al. 2011; Lin et al. 2006; Haufe et al. 2011), yet there are hardly any studies that have directly assessed the impact of method selection on the subsequent source-level coupling analysis (cf. Schoffelen & Gross 2009; Hui et al. 2010).

Because MNE and spatial filters are widely used inverse solutions in MEG, it would be helpful to understand whether they differentially impact source-level connectivity estimations and, in particular, what parameters affect their potential difference in performance. Although beamformers are by construction tuned to work with uncorrelated sources, they have been shown to be stable to moderately correlated sources and to even localize completely correlated point-like sources in the presence of noise (Van Veen et al. 1997; Gross et al. 2001;

Hadjipapas et al. 2005; Sekihara et al. 2005; Küçükaltun-Yildirim et al. 2006; Kujala et al. 2008; Quraan & Cheyne 2010). Given that this assumption about uncorrelated sources is embedded in beamformer reconstructions, one may ask how it affects the identification of coherent sources, compared to inverse solutions that do not make such an assumption (for instance MNE)? Furthermore, how do the connectivity-detection performances of MNE and beamforming compare when the coupled sources vary in size, or in coupling strength? And how does the noise level affect the performance of both methods when it comes to detecting interacting sources? These are all open questions which we address here via extensive data simulations.

More specifically, the goal of the current study is to investigate the effect of the inverse method selection on the quality of subsequent source-space connectivity analyses. In particular, we evaluated the difference in the ability to correctly uncover oscillatory coupling in source-space following an initial source estimation step that is either performed with (a) Minimum Norm Estimate (MNE), (b) Linearly Constrained Minimum Variance (LCMV) beamformer or (c) Dynamic Imaging of Coherent Sources (DICS) beamformer. This was achieved using numerous simulations of oscillatory signals where we varied a range of parameters, including source size, inter-patch and intra-patch coherence strengths and signal-to-noise ratio (SNR).

2. Methods and Materials

Although our main objective is to evaluate the effect of using different methods to estimate coherence between cortical areas, we also compare the performance of the methods to localize active sources by evaluating their accuracy in determining the levels of oscillatory power. This power estimation also allows us to compare our results with other studies. For the analysis with MNE and LCMV, the time-series of the signals are first reconstructed and then spectral coherence and power can be calculated. DICS operates in the frequency domain allowing for a direct reconstruction of coherence and power. As shown in section 2.3 and 2.4,

LCMV and DICS beamformers are based on the same filtering principle, but DICS was especially designed to detect coherent sources and has the advantage of a very low computational cost. In this section, we first define the inverse methods used and then describe the simulation, reconstruction and performance assessment procedures.

2.1 The MEG Inverse Problem

The inverse solution seeks to identify an estimate of the active sources **S** ($3n_{\text{sources}}$ x *time points*) that generate the measurements **M** (n_{channels} x *time points*) recorded at the sensors. The dimension $3n$ of the columns of **S** accounts for the three components of the source n in the x, y and z directions. According to anatomical observations, the main generators of MEG are located in the grey matter and their orientation is perpendicular to the cortical sheet (Nunez & Srinivasan 2006). Here, we used a constrained orientation approach (elemental dipoles perpendicular to the cortical surface), and the dimensions of $\boldsymbol{S}$ are therefore reduced to (n_{sources} x *time points*). Assuming a linear relationship between the measurements and the active sources, the problem can be modeled as:

$$\mathbf{M} = \mathbf{LS} + \mathbf{N} \qquad (1)$$

where **L** is the Lead field matrix (n_{channels} x n_{sources}) and **N** is additive noise applied at the MEG channels (n_{sources} x *time points*). The lead field matrix describes how each source contributes to the measurements at each sensor, given a specific head conductivity model and a source space. As the number of sources is typically much higher than the number of sensors, the lead field matrix is highly underdetermined and thereby not invertible. The estimation of the activity of the sources requires the definition of an inverse operator **W**:

$$\hat{\mathbf{S}} = \mathbf{W}^T\mathbf{M} \qquad (2)$$

where $\hat{\mathbf{S}}$ represents the estimated sources (n_{sources} x *time points*) and the superscript T denotes matrix transpose.

2.2 Minimum Norm Estimate (MNE)

Since the MEG inverse problem is ill-posed, a regularization scheme is needed (Hämäläinen & Ilmoniemi 1984; Hämäläinen & Ilmoniemi 1994). The most common options are SVD truncation or Tikhonov regularization (Tikhonov & Arsenin 1977; Foster 1961). MNE calculates an inverse operator **W** by searching for a distribution of sources $\hat{\mathbf{S}}$ with minimum

currents (L2-norm) that produces an estimation of the measurements ($\mathbf{L\hat{S}}$) most consistent with the measured data ($\mathbf{M}$). The solution is a trade-off between the norm of the estimated regularized source currents $\lambda^2\|\mathbf{\hat{S}}\|^2$ and the norm of the quality of the fit they provide to the measurements $\|\mathbf{M}-\mathbf{L\hat{S}}\|^2$. If we assume the noise $\mathbf{N}$ and the source strengths $\mathbf{S}$ to be normally distributed with zero mean and covariance matrices $\mathbf{Q}$ and $\mathbf{R}$ respectively, a general form of the MNE inverse solution is given as (Dale & Sereno 1993; Dale et al. 2000; Lin et al. 2004):

$$\mathbf{\hat{S}} = \mathrm{argmin}_S\left\{\left\|\mathbf{Q}^{-1/2}(\mathbf{M}-\mathbf{LS})\right\|^2 + \lambda^2\left\|\mathbf{R}^{-1/2}\mathbf{S}\right\|^2\right\} \qquad (3)$$

where λ is the Tikhonov regularization parameter, $\mathbf{Q}$ the noise covariance matrix, and $\mathbf{R}$ the source covariance matrix. The inverse operator $\mathbf{W}$ is thus defined as:

$$\mathbf{W} = \mathbf{RL}^T(\mathbf{LRL}^T + \lambda^2\mathbf{Q})^{-1} \qquad (4)$$

where the superscript *-1* denotes matrix inverse.

In a previous study, we used the same simulation procedure to investigate whether the optimal minimum-norm regularization coefficient to estimate coherence was identical to the optimal one for power estimation (Hincapié et al. 2016). The mean optimal Tikhonov regularization coefficient for coherence detection turned out to be, in fact, two orders of magnitude lower than the one needed for power detection. This is largely due to the fact that increased regularization (i.e. smoothing) blows up the rate of false positives, a problem that appears to be amplified for cortico-cortical coupling (Hincapié et al. 2016). Therefore, in the current study, we used the mean optimal regularization parameters reported previously (i.e., 1e-9 for coherence estimations and 1e-7 for power estimations). Note that, as the two terms in equation (3) are in the same units (fT/cm or fT), the regularization factor lambda has no unit. Moreover, when available, spatial priors can be incorporated in $\mathbf{R}$ (Mattout et al. 2005; Phillips et al. 2005). As we chose not to use priors, here $\mathbf{R}$ is the Identity matrix. The noise covariance matrix $\mathbf{Q}$ was computed from the actual noise which was added to the sensors in each simulation.

2.3 LCMV Beamforming

The LCMV beamformer looks for signals coming from a few active but uncorrelated regions of unknown location. The inverse operator **W** is a set of spatial filters, calculated at each source location (**r**), to pass the signal from that location while suppressing signals from other locations. The operator **W** minimizes the variance at the filter output subject to a linear constraint. This variance minimization assures the stopband response to be small at a location different to the one being filtered. The output variance or power of each filter (therefore at each source location) provides the estimation of the activity in the brain (Van Veen et al. 1997). This is formulated as follows:

$$\textbf{Variance}\ (\mathbf{r}) = \text{trace}\left[\mathbf{W}^T(\mathbf{r})\mathbf{C_m}^{-1}\mathbf{W}(\mathbf{r})\right] \quad (5)$$

$$\min_{\mathbf{W}(\mathbf{r})}\ \text{trace}\left[\mathbf{W}^T(\mathbf{r})\mathbf{C_m}^{-1}\mathbf{W}(\mathbf{r})\right]\ \text{subject to}\quad \mathbf{WL}(\mathbf{r}) = \mathrm{I} \quad (6)$$

Minimizing the corresponding Lagrangian function, the solution obtained is:

$$\mathbf{W}(\mathbf{r}) = \left(\mathbf{L}^T(\mathbf{r})\mathbf{C_m}^{-1}\mathbf{L}(\mathbf{r})\right)^{-1}\mathbf{L}^T(\mathbf{r})\mathbf{C_m}^{-1} \quad (7)$$

Where $\mathbf{C_m}$ is the data covariance matrix. Inserting eq. (7) in eq. (2) gives an estimate of the signal at each location of interest **r**. This estimate of the signal is usually normalized by the estimated noise which van Veen et al. (1997) termed the neural activity index. The estimated noise signal at each location is calculated in analogy to the estimated signal, but replacing the data covariance matrix $\mathbf{C_m}$ by the noise covariance matrix **Q**. Note that we used a standard unregularized LCMV approach.

2.4 DICS Beamforming

DICS has the same filtering principle than the LCMV, but it works in the frequency domain and uses regularization to tune the resolution of the reconstructions (Gross et al. 2001). The filter is defined as:

$$\mathbf{W}(\mathbf{r}, f) = \left(\mathbf{L}^T(\mathbf{r})\mathbf{C_r}(f)^{-1}\mathbf{L}(\mathbf{r})\right)^{-1}\mathbf{L}^T(\mathbf{r})\mathbf{C_r}(f)^{-1} \quad (8)$$

where $\mathbf{C_r}(f) = \mathbf{C}(f) + \alpha \mathrm{I}$, and $\mathbf{C}(f)$ is the cross spectral density matrix at frequency f (or averaged across a frequency band centered at f) and $\boldsymbol{\alpha}$ is a regularization parameter (its value is relative to the largest singular value in the data).

The cross spectrum estimates at locations $\mathbf{r_1}$ and $\mathbf{r_2}$ at frequency f are calculated by:

$$\mathbf{Cs}(\mathbf{r}_1, \mathbf{r}_2, f) = \mathbf{W}(\mathbf{r}_1, f)\mathbf{C}(f)\mathbf{W}^T(\mathbf{r}_2, f) \qquad (9)$$

When $\mathbf{r_1}$=$\mathbf{r_2}$, $\mathbf{Cs}$ is the power estimate matrix. Noise normalization is done as described for the LCMV. The cross spectrum estimates from equation (9) are used to calculate power and coherence as described by equations (10) and (11) in section 2.6.

2.5 MEG data simulation

We simulated oscillatory activity in pairs of cortical sources with various levels of coupling in the alpha frequency band (9-14 Hz). We calculated the resulting sensor-level data through forward modeling based on a 275 channel CTF MEG system configuration. The simulated sources consisted of current dipoles placed at the vertices of a MNI-Colin 27 cortical surface, which was segmented and tessellated using FreeSurfer (Fischl 2012), and down-sampled to 15028 vertices. Different strengths of coupling were obtained by forcing the time series of the two simulated source to have a certain level of coherence. We calculated the fields at the sensors using a single sphere head model and constraining the orientations of the sources to be normal to the cortical surface. The simulated data were generated using a combination of custom code written in MATLAB (Mathworks Inc., MA, USA) and functions from Brainstorm (Tadel et al. 2011) and FieldTrip (Oostenveld et al. 2011) toolboxes.

The source time courses were simulated by first setting the base frequency of the two oscillators (e.g. 12 Hz), and by inducing small, random jitters to the instantaneous frequencies of both oscillators at each time point. Both oscillators consisted of 70000 samples (i.e. approx. 117 seconds, given a 600 Hz sampling frequency). The jittered instantaneous frequencies were then used to generate the sine wave oscillators using an exponential function and the cumulative sums of the instantaneous frequencies (Appendix A contains an algorithmic

description of the equation used to generate such time series). In practice, this approach generates two oscillators that operate on average at the same frequency (e.g. 12 Hz) and start off with a zero-phase lag. However, as the frequencies of the oscillators are jittered across time, the instantaneous phase relationship also fluctuates between positive and negative values. As the phase relationship between the two oscillators is not constant, the procedure allows us to achieve coherence levels below 1. The frequency jittering was performed randomly in a loop until the desired coherence level (e.g. 0.4) between the time courses of the two oscillators was obtained. The Matlab code developed to generate the coupled oscillatory time series has been made available online via github (see https://github.com/ahincap/create-coherent-time-series/tree/master). Futhermore, the formula used to generate each oscillatory time series is provided in Appendix A.

We randomly selected two locations (seeds) for each simulated pair of sources (600 pairs). For each pair, we then varied the following three parameters in the simulations: (a) the spatial extent of the sources, (b) the strength of the coupling between the two sources and finally, (c) the signal-to-noise ratio (SNR) at the sensors. For a subset of source configurations, we also varied the intra-patch coherence levels, i.e. the coupling between elemental dipole time courses belonging to the same patch. These parameters are described in more detail below:

(I) Patches and point-like sources: We simulated point-like sources (i.e. 1 dipole) and cortical patches (with surface areas of 2, 4 or 8 cm^2). Note that the activity of a cortical patch was simulated by generating multiple identical time series at the vertices that make up the patch. As a result, dipoles within a single patch were perfectly coherent. Patches with lower intra-patch coherence were also simulated (see IV below).

(II) Coupling strength: The time series of elemental dipoles of the interacting pairs of sources were generated such that the alpha-band coherence was 0.1, 0.2 or 0.4. The simulated time series were 7000 samples long (600 Hz sampling frequency). Note here that because we actually simulate coherence at the source level, we subsequently assess the ability of the methods to recover truly coherent cortico-cortical activations. In other words, although ambiguities may arise from field spread effects, we do know by construction that the underlying generators are truly coherent.

(III) Signal to Noise Ratio (SNR): Three levels of SNR (0 dB, -20 dB and -40dB) were obtained by adding Gaussian uncorrelated noise to the sensor signals. The SNR was calculated as the ratio of the Frobenius norm of signal and noise amplitudes at the sensors.

(IV) Partly-coherent patches: To take into account the putative effect of intra-source time series coherence on inter-source coherence estimation, we also simulated patches where intra-patch coherence was reduced (mean intra-patch coherence across conditions was 0.2, instead of the 1.0 intra-patch coherence for all previously described simulations). The mean intra-patch coherence is computed by taking the mean of coherences calculated across all possible pairs of dipoles between the two patches. These partly-coherent patches were simulated in 50 configurations of pairs of sources with the inter-mediate patch size of 2 cm^2, three levels of SNR (0, -20 and -40dB) and inter-seed coherence value of 0.2 (i.e. coherence between the time series of the seeds of the two patches). These configurations are thus best described by three coherence measures: inter-seed coherence, intra-patch coherence and inter-patch coherence.

(V) Inter-source distance: The putative effect of the distance between the two interacting sources on the connectivity estimation was also investigated. Although we did not specifically manipulate inter-source distance as a simulation parameter, we were able to evaluate the performance of connectivity detection as a function of inter-areal distance by plotting the performance as a function of inter-source distance across all simulated configurations (using linear regression). This was performed for each of the three reconstruction methods tested and for point-like sources and patches.

To summarize, 600 different pairs of source locations were randomly chosen across the cortex and used to calculate MEG sensor data. The time series in each pair were manipulated to generate various inter-source coupling strengths (3 levels: 0.1, 0.2 or 0.4) and source sizes were set to range across 4 levels (from point-like to 2, 4 or 8 cm^2). Three levels of sensor-level SNR were used (0 dB, -20 dB and -40dB). Moreover, we also generated 50 additional configurations where the simulated coherence between the time series that make up each single patch (intra-patch coherence) was lowered to 0.2 on average. In this control condition, we fixed inter-seed coherence to 0.2, patch size to 2 cm^2 and we used three SNR levels (0, -20 and -40dB). In total, we created 21900 sets of simulated MEG sensor-level data

2.6 Power and Coherence Reconstructions

Once the MNE and LCMV time series and the DICS cross-spectral density matrix were calculated, we estimated source-space spectral power (at any location **r**) and magnitude squared coherence (between two locations $\mathbf{r_1}$ and $\mathbf{r_2}$) as follows

$$\mathbf{P}(\mathbf{r}, f) = \mathbf{Cs}(\mathbf{r}, \mathbf{r}, f) \quad (10)$$

$$\mathbf{Coh}(\mathbf{r}_1, \mathbf{r}_2, f) = |\mathbf{Cs}(\mathbf{r}_1, \mathbf{r}_2, f)|^2 / (\mathbf{P}(\mathbf{r}_1, \mathbf{r}_1, f)\mathbf{P}(\mathbf{r}_2, \mathbf{r}_2, f)) \quad (11)$$

where **Cs** is the cross-spectral density matrix, and f the frequency bin. Power and MS coherence were calculated via built-in standard MATLAB functions based on Welch's averaged and modified periodogram method (Welch 1967). For coherence, we used a seed-based approach where the reconstructed time series at one of the two simulated sources was used as reference, and we calculated its coherence with all other source time series across the brain.

2.7 Receiver Operating Characteristic (ROC) Curves

The performance of each method was evaluated using the area under the curve (AUC) from the ROC curves which are obtained by plotting the True Positive Fraction (TPF) against the False Positive Fraction (FPF) at variable threshold levels α:

$$TPF(\alpha) = TP(\alpha)/Number\ of\ simulated\ dipoles \quad (12)$$

$$FPF(\alpha) = FP(\alpha)/(Total\ number\ of\ dipoles - Number\ of\ simulated\ dipoles) \quad (13)$$

where $TP(\alpha)$ represents the true positives (i.e. the intersection between simulated sources and active sources at threshold α) and $FP(\alpha)$ represents the false positives (i.e. all active sources excluding the true positives at activation threshold α). By computing *TPF* and *FPF* repeatedly for successive values of activation thresholds α we obtain the standard ROC curve. The AUC derived from the ROC curve is taken as a measure of performance, i.e. higher AUC

indicates higher performance. Statistical comparisons between AUC measures for the various methods across all configurations were performed using standard two-tailed t-tests.

Note that for reference-based coherence reconstruction, computing true positives can be ambiguous if we consider the sources within the "reference patch" (location 1) to be true positives. Since we are primarily interested in assessing how well the distant coherent patch (location 2) is detected, we used the time series estimated at location 1 -as a seed- and considered only the simulated connectivity that make up the patch at location 2 to be the vertices we wish to detect (*TP*).

Control for bias towards FPF:

A potential problem in the ROC-based performance evaluation could in theory arise from the fact that the number of vertices in the source space (total number of dipoles) exceeded by far the number of active sources in our simulations (true positive dipoles). We used a source space grid of 15028 vertices (total number of dipoles) and our simulations consisted of dozens of simulated dipoles (60 dipoles for the largest patches), which can generate a bias towards the *FPF*. To investigate this, we randomly sampled a number of non-active dipoles (*TN*) equal to the number of simulated dipoles (*TP*) and calculated the *TPF* and the *FPF*. In other words, for a true active patch of, for instance 60 dipoles, we randomly selected 60 dipoles from the *TN*, and used the activity values of these 120 dipoles for the ROC/AUC calculation. This allowed us to enforce a balance between *TP* and *TN*. This procedure was repeated 100 times for each *TP* patch. The resulting 100 AUC values were averaged to get a representative AUC for each configuration. A set of 50 source configurations was used in this analysis. This control analysis yielded AUC measures that are extremely close to the those obtained with the standard approach (see result section 3.5 and Table 1 for details).

Control for spatial smoothing (source blur)

Lastly, we analyzed the potential effect of seed blur (spatial smoothing) on the AUC performance metric. To this end, we asked whether a less conservative definition of the *TPF* would have an effect on the evaluation of the methods. To this end, we performed the analysis by including neighboring vertices (around the simulated source) in the definition of true positives. The pseudo true positives were defined as all vertices within a source patch 3 times bigger than the actual simulated patches (e.g. for a 2 cm^2 patch, all dipoles with a 6 cm^2 patch, centered on the same vertex, were all considered pseudo true positives). In this control

analysis, we also took into account the bias towards *FPF* (cf previous section). As in the previous section, we used a subset of 50 configurations in this analysis. We found that the less conservative definition of the *TPF* did not affect the results (See section 3.5 and Table 1 for details).

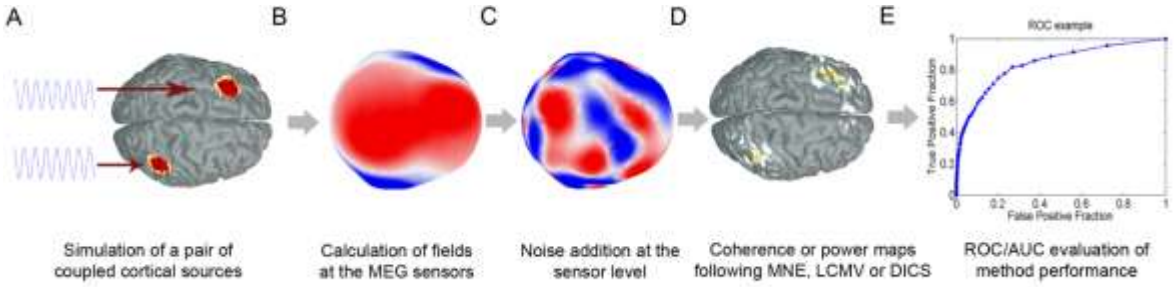

Figure 1. Overview of the simulation and analysis pipeline that was developed in this study to **(A)** create pairs of coherent cortical patches, **(B)** generate the corresponding MEG sensor data through forward modeling, **(C)** add noise, **(D)** reconstruct the underlying sources and calculate power or coherence maps, and **(E)** evaluate the detection performance using ROC curves and AUC, for a given inverse method.

3. Results

In this section, we first describe the average results for the methods comparison; second and third, we show the effect of the SNR and the strength of coupling on the performance of the methods and lastly, we show the effect of low intra-correlation of the patches on the performance of the methods. As the size of the sources has an important effect on the performance of the three methods, we present the results separately for point-like (two coupled single-dipole sources) and for cortical patches.

3.1 Methods Comparison: MNE, LCMV and DICS

Globally, beamformers (LCMV and DICS) have a similar performance in all cases (there are no statistically significant differences between them) and, have a statistically significant ($p<0.001$) higher performance than MNE for power reconstructions and coherence reconstructions for point-like source configurations (Figure 2B, 2C and 2D). However, MNE provides better coherence performance than beamformers for the cortical patches (Figure 2A). The drop in beamformer performance when detecting interacting patches (compared to identifying interacting point-like sources) is most likely due to the fact the identical elemental dipole time series within a single patch give rise to more signal cancellation.

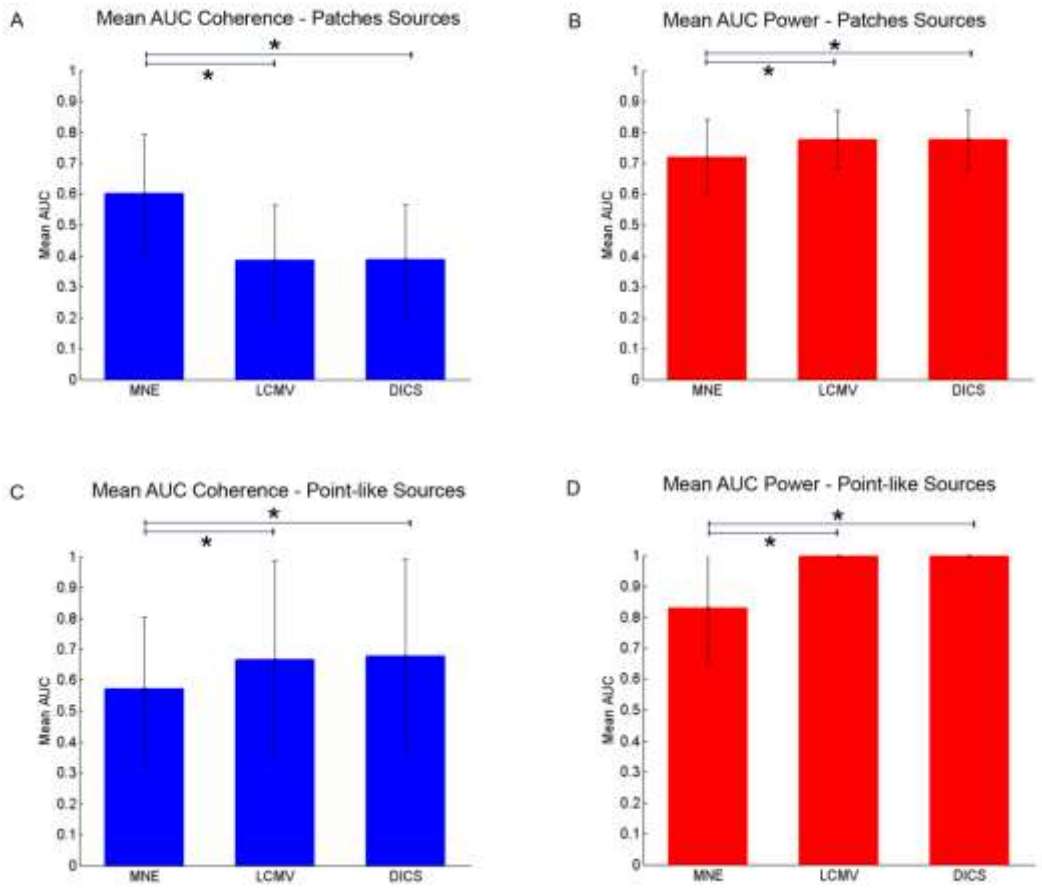

Figure 2. Performance comparison for coherence and power detection using all three inverse methods. **(A)** Mean AUC for coherence reconstructions of cortical patches (* indicates statistically significant differences at p<0.001, t-test). **(B)** Mean AUC for power reconstructions of cortical patches. **(C)** Mean AUC for coherence reconstructions of point-like sources. **(D)** Mean AUC for power reconstructions of point-like sources.

3.2 Effect of SNR

Regarding the effect of SNR on coherence reconstructions of patch simulations, MNE shows higher AUC values that expectedly decrease with decreasing SNR. There is a statistically significant effect of the values of SNR for MNE (p<0.001, t-test), but not for the beamformers (Figure 3A). For power reconstructions, although SNR has a statistically significant effect on the three methods, beamformers are more stable to different values of SNR and have a statistically significant higher performance than MNE (Figure 3B and 3D). For the highest SNR condition (0dB), MNE has a higher performance (p<0.001, t-test) than the filters for

coherence reconstructions of point-like sources and for power reconstructions of cortical patches (Figure 3A and 3D). For the lowest SNR condition (-40dB), DICS has the best performance for coherence reconstructions of point-like sources. The lower performance of MNE at 0dB for reconstructions of point-like sources is explained by the use of the average optimal lambda, which is one order of magnitude larger than the optimal value for these conditions. For the beamformers, the decrease in performance at the 0dB condition for point-like sources is due to the fact the beamformers are spatially extremely focal at this SNR. As the maximum output for the beamformers was not always on the exactly right vertex, this led for many source configurations to a lower performance than at the lower SNR conditions. Note that as the SNR has been defined from the raw simulated signals, the effective SNRs at the studied, narrow frequency band are, in fact, about 20dB higher than what are given in the definitions (Fig 3D).

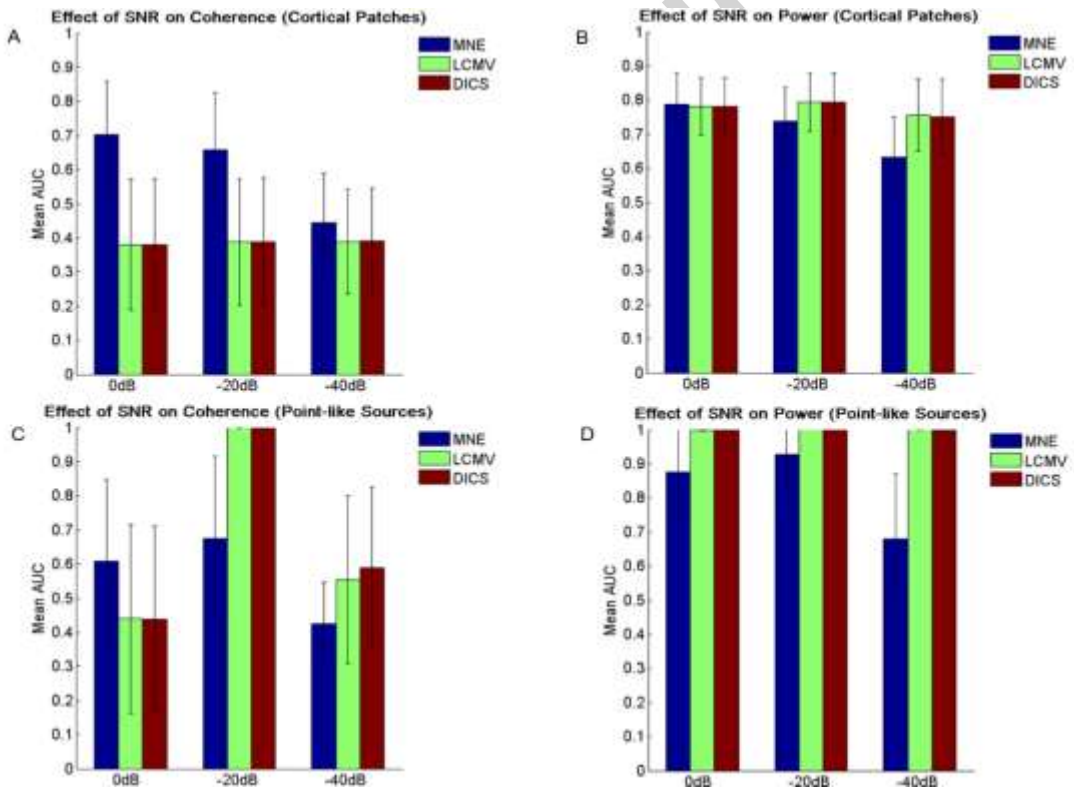

Figure 3. Effect of SNR on coherence and power reconstructions. **(A)** Effect of SNR on coherence for coupled patches (extended sources). **(B)** Effect of SNR on power for patch sources. **(C)** Effect of SNR on coherence for point-like sources. **(D)** Effect of SNR on power for point-like sources.

3.3 Effect of strength of coupling

According to the statistical analysis, there is a significant difference between the performances obtained with coupling strengths of 0.1 and 0.4 for beamformer power and coherence reconstructions of point-like sources. The reconstructions at 0.1 coupling have a better performance than those at 0.4 coupling for power reconstructions (Figure 4D). In contrast, the reconstructions at 0.4 have a better performance for coherence reconstructions (Figure 4C). There is no effect of the strength of coupling for the MNE power reconstructions (Figures 4B and 4D), but there is a significant effect for coherence reconstructions, showing higher AUC values that expectedly increase with increasing coherence between the simulated sources (Figures 4A and 4C).

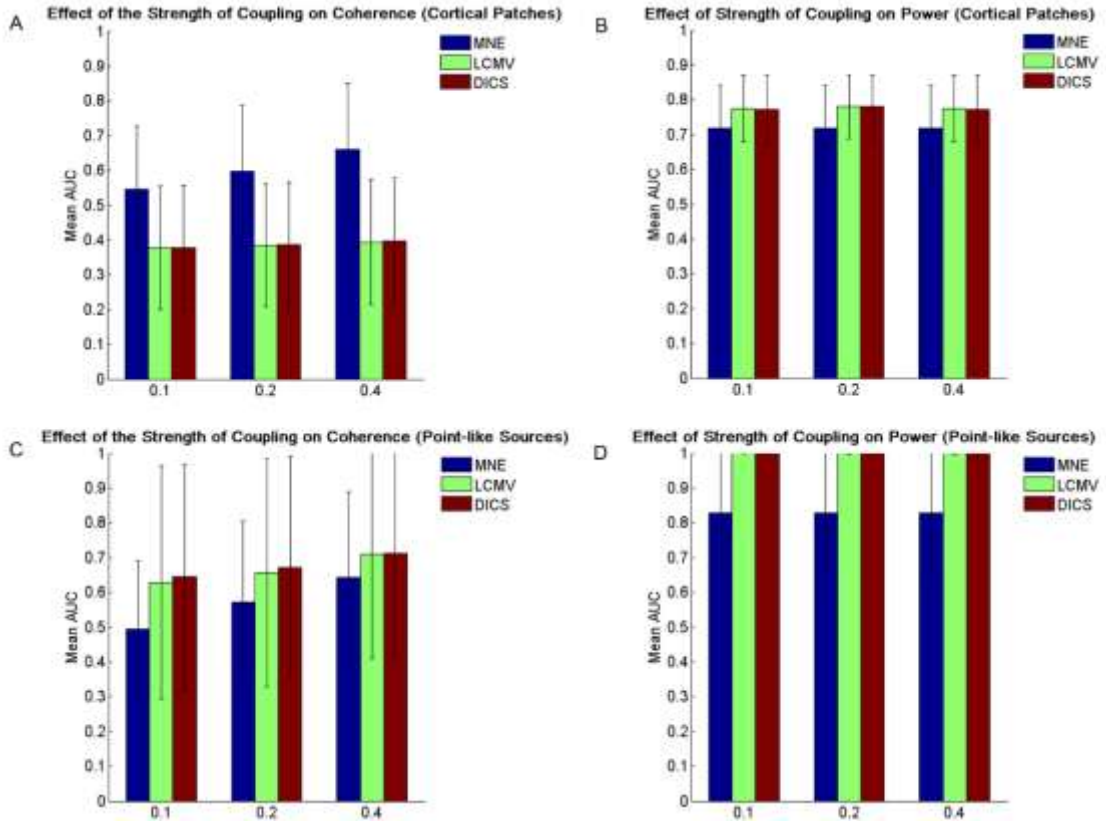

Figure 4. Effect of inter-source coherence strength (Coh=0.1, 0.2 and 0.4) on coherence and power reconstruction results (mean AUC) with each of the three methods. **(A)** Effect of strength of coupling on coherence detection for patch sources. **(B)** Effect of strength of coupling on power detection for patch sources. **(C)** Effect of strength of coupling on coherence detection for point-like sources (single dipole). **(D)** Effect of strength of coupling on power detection for point-like sources.

3.4 Results with alternative ROC performance metrics

As described in section 2.7, we also used two modified approaches to the standard ROC in order to control for bias towards *FPF* (i.e. due to the imbalance between *TN* and *TP* in our simulated data) and for spatial smoothing (source blur). Table 1 shows the mean AUC for a subset of 50 configurations obtained with the standard approach (Method 1) and with the modified methods (Methods 2 and 3). The results indicate that the two modified ROC/AUC methods did not have a substantial effect on the mean AUC for coherence detection, neither for the patches nor for point-like configurations. Interestingly, the mean AUC obtained with patches using beamforming were below 0.5, which is in theory an indicator that the method performs below chance levels. This intriguing observation cannot be simply explained by the imbalance between true positives and true negatives because it was observed with all three ROC/AUC methods used here. A likely explanation is the full correlation between the times series of the elemental dipoles that make up each patch and the way this adversely impacts the beamformer approach, through signal cancellation. This issue is tackled in the next section.

Table 1. Summary of mean method performance for coherence and power detection using standard and modified ROC/AUC approaches. Method 1: standard FPF-TPF ROC/AUC methodology. Method 2: Modified ROC/AUC controlling for the large imbalance between TN and TP. Method 3: Modified ROC/AUC taking into account spatial resolution or seed blur (by expanding the true positive set to include neighboring vertices) and controlling for the large imbalance between TN and TP. (See section 2.7 for details).

	Inverse Method	**Patches Mean AUC (±std)**	**Point-like sources Mean AUC (±std)**
Method 1 Standard ROC/AUC	MNE	0,6145 ±0,1953	0,5730 ±0,2387
	LCMV	0,3822 ±0,1851	0,6750 ±0,3141
	DICS	0,3824 ±0,1861	0,6853 ±0,3064
Method 2 Modified ROC/AUC Control for imbalance between TN and TP	MNE	0,6145 ±0,1955	0,5746 ±0,2416
	LCMV	0,3821 ±0,1851	0,6765 ±0,3148
	DICS	0,3825 ±0,1860	0,6847 ±0,3076
Method 3 Modified ROC/AUC Control for spatial resolution (seed blur) and TN/TP imbalance	MNE	0,6052 ±0,1850	0,5510 ±0,2085
	LCMV	0,3844 ±0,1680	0,6081 ±0,2569
	DICS	0,3842 ±0,1688	0,6186 ±0,2510

3.5 Effect of intra- patch coherence

As beamformers assume no correlation between the sources to be reconstructed, high within-patch coherence (such as identical time series across the vertices of a single patch) is expected to adversely affect the results of beamformer coherence detection. This is a likely explanation of the results above where DICS and LCMV were outperformed by MNE for the detection of coupling among interacting patches, where each patch was made up of multiple identical time series). When the within-patch coherence was forced to be substantially lower than 1 (mean intra-patch coherence of 0.2), the connectivity performance of the beamformers significantly improved (Figures 5). MNE coherence reconstructions were not affected by the reduction in within-patch coherence. Our findings confirm that total intra-patch coherence for extended patches impeded the coherence detection performance of beamformers.

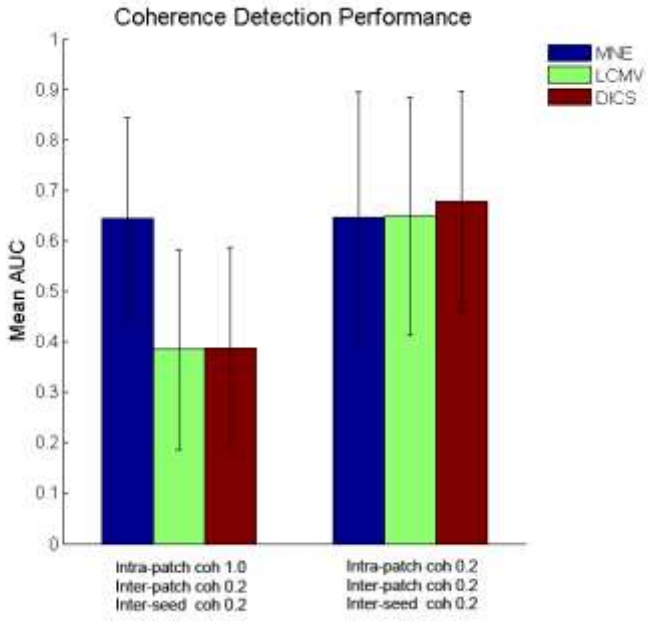

Figure 5. Comparison of results obtained with fixed between-patch coherence (i.e. inter-patch coh=0.2) but variable within-patch coherence (i.e. intra-patch coh= 1.0 or 0.2). Bar plots show mean AUC for coherence detection for coupled patches of 2 cm^2. Left column correspond to cases of fully coherent patch time series, i.e. all dipoles inside each patch are fully coherent (i.e. intra-patch coherence =1.0) and the right column represents results of partly coherent patch time series (intra-patch coherence set

to 0.2). The right columns depict the positive effect of reduced intra-patch coherence on beamformer performance. The performance of MNE remains stable.

Figure 6 illustrates the effect of (i) inverse method selection and (ii) changes in intra-patch coherence on the detection of MEG cortico-cortical coupling. The simulated configuration (Fig 6A) shows a pair of cortical patches (one on each hemisphere), with inter-patch coherence strength set to 0.2, patch size to 2 cm^2 and SNR to -20dB. Figure panels 6B and 6C show the obtained cortical coherence maps estimated with respect to the reference seed (indicated in panel A), after using each one of the 3 inverse methods. In Fig 6B the simulated dipole time series inside each patch are entirely coherent (intra-patch coherence set to 1, *Config 1*), while in 6C, the time series of the dipoles that make up each patch were forced to have lower coherence (intra-patch coherence set to 0.2, *Config 2*).

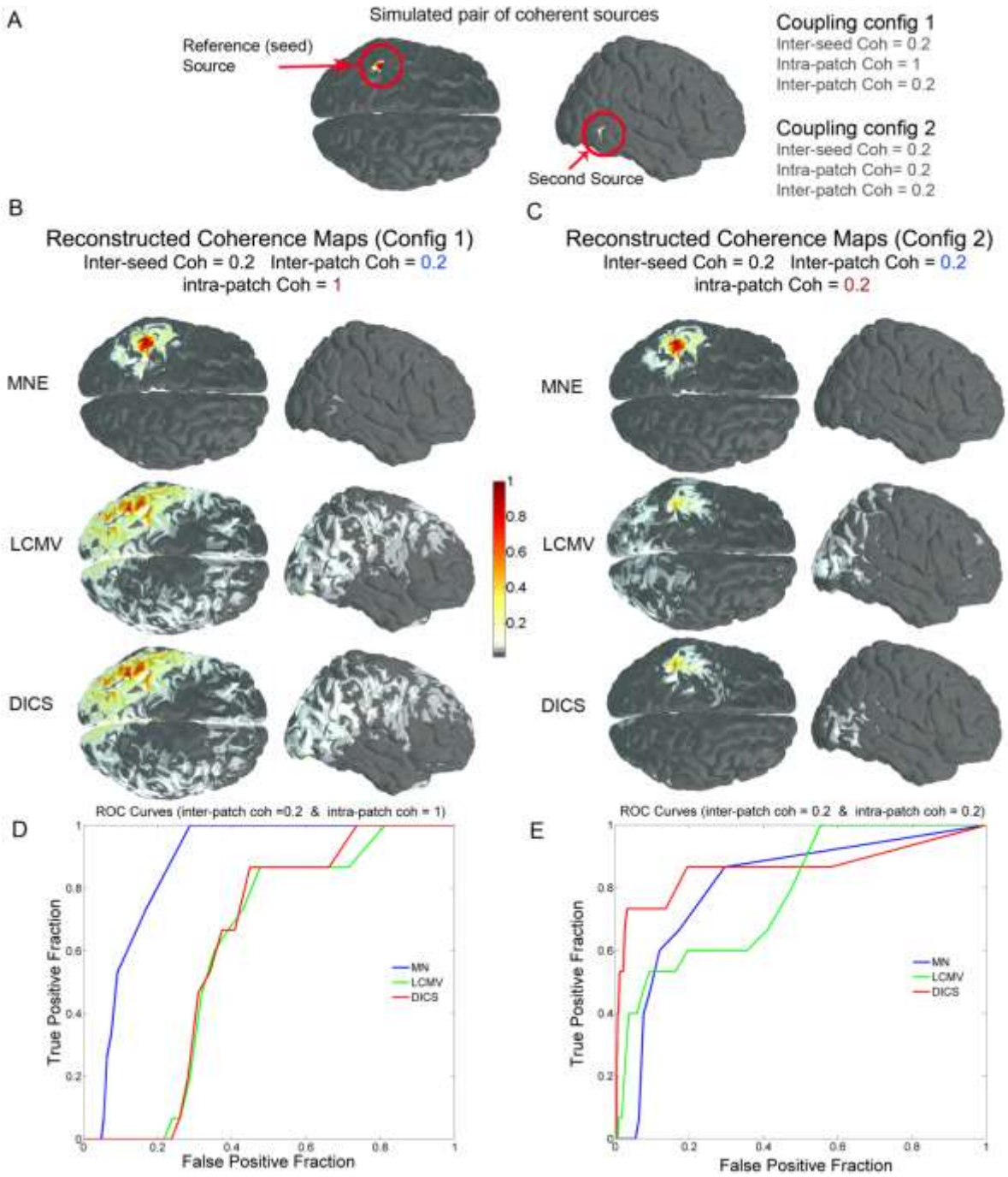

Figure 6. Illustrative examples of the effect of inverse method, and intra-patch coherence on the detection of MEG cortico-cortical coupling. **(A)** Illustrative configuration of simulated alpha-band long-range cortico-cortical coherence (patch size=2 cm^2, inter-patch coh=0.2, SNR=-20dB). The coherence among the time series of dipoles inside each single patch were either totally coherent (intra-patch coherence =1, Config 1), or only partly coherent (intra-patch coherence=0.2, Config 2). **(B)** Reconstructed coherence maps for Config 1, obtained using source 1 as seed (see panel A), and with the three inverse methods (MNE, LCMV and DICS). **(C)** Same as Panel (B) but for Config 2 (i.e. mean intra-patch coherence reduced to 0.2 while the inter-patch and inter-seed coherences were both maintained at 0.2). The maps in B and C are thresholded at 0.01, and extend up to 1, i.e. max coherence. **(D,E)** Standard ROC-curves for each method corresponding to the coherence results in (B,C), respectively (see Methods section for details).

Figure 6B, and the associated ROC curves in Fig 6D, illustrate how MNE can outperform the beamformer for coherence detection when the individual dipole time series that make up each single patch are all coherent (identical time series). Note here, that the inter-patch coherence (i.e. cortico-cortical coupling) and the inter-seed coherence here was 0.2. The beamformer reconstructions of coherence were associated with a high false positive fraction. Although MNE coherence reconstruction also depicts a relatively high false positive fraction, the highest reconstructed values are located around the true location of the sources, giving rise to a true positive fraction that remains high through all the ROC threshold sampling steps. These differences yield lower AUC values for DICS and LCMV compared to MNE. The results differ substantially for configuration 2 (Figures 6C and 6E). Here, coherence reconstructions using both LCMV and DICS clearly improve because of the lower intra-patch coherence (0.2, instead of 1.0 as in Fig 6B,D). This is likely due to the fact that the beamformer performance was hindered in configuration 1 by the presence of fully correlated time series inside each patch (intra-patch coherence =1). In contrast, the performance of MNE slightly dropped in configuration 2. This could be due to the use of a regularization parameter lambda that is optimal for fully coherent patches, and is sub-optimal here. It is very important to keep in mind that the examples shown in figure 6 are just configurations that we chose to illustrate and visualize aspects that are representative of the global findings obtained across all the simulations (see for example Figure 5). One may very well find configurations that show different results.

3.6 Effect of inter-source distance

The investigation of the impact of inter-source distance on connectivity performance suggests that the distance between sources has little if any effect on connectivity performance when the interacting sources are modeled as point-like sources (Fig 7A). Yet, when it comes to pairs of coupled cortical patches, beamformers show a decrease in performance (quantified by AUC) with increasing inter-source distance (Fig 7B). As shown in Fig 7C, this effect was weaker, though still present, when the individual dipole time series within each patch were simulated with low coherence (intra-patch coh =0.2). The interpretation of these observations is non-trivial. One cannot rule out, that factors such as the specific geometry of the distant

sources provide conditions that are less favorable for the beamformer approach (e.g. more vulnerable to signal cancellation). Most importantly, however, as shown in Fig 7C, the observed effect of inter-source distance is clearly reduced for partially coherent patches. Thus, the inter-source distance seems to affect the beamformer connectivity performance only in scenarios where there is a massive amount of correlated activity present in spatially extended patches, potentially leading to a violation of the beamforming principles. A more systematic simulation analysis tailored to determining the effect of inter-source distance would be needed, to fully and adequately address this question.

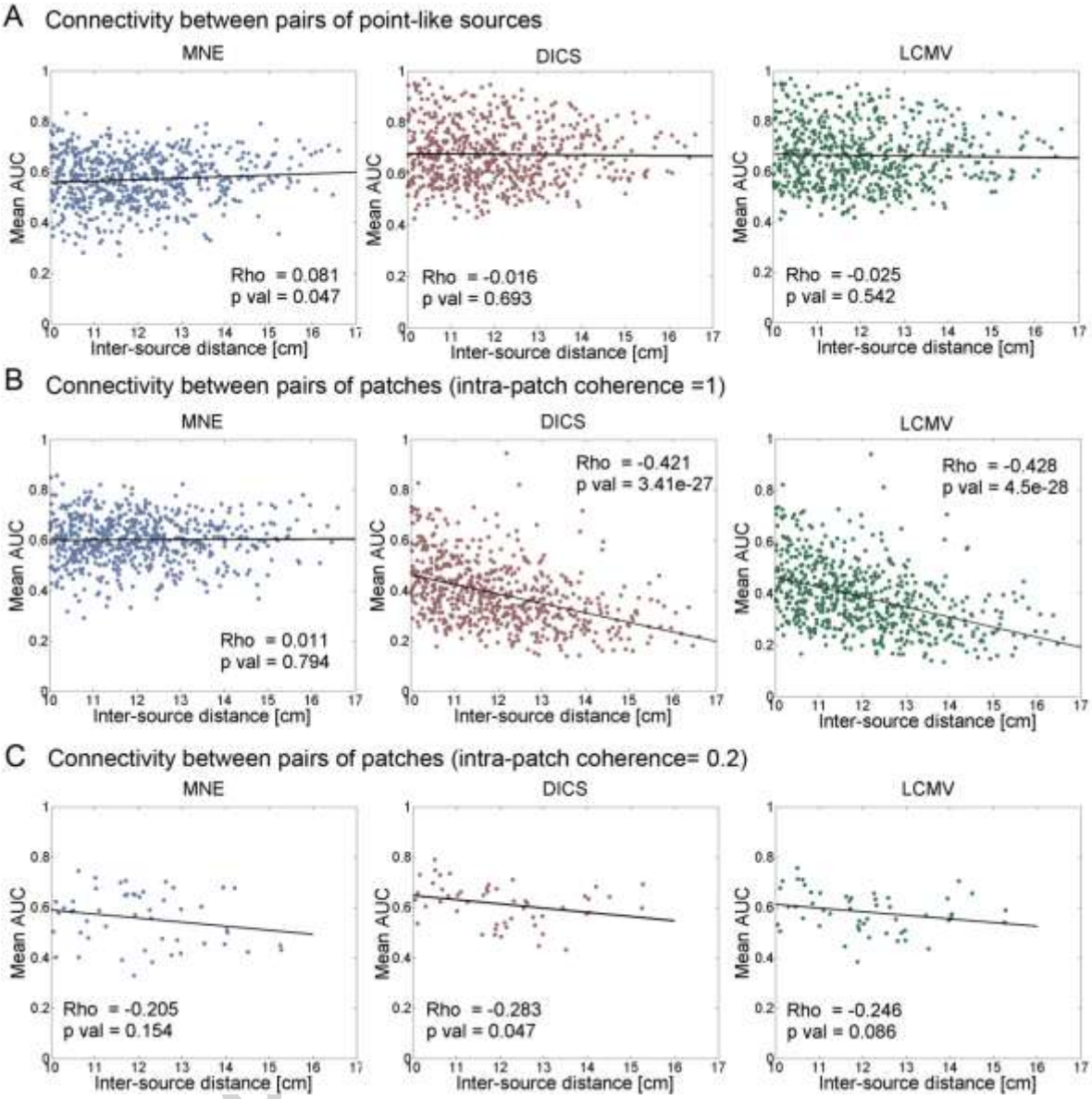

Figure 7. Effect of inter-source distance on connectivity estimation performance, for MNE, DICS and LCMV. (A) Effect of source distance on connectivity estimation performance when using pairs of point-like sources (mean AUC across 3 coupling strengths and 3 SNR values i.e. 9 combinations for each of 600 pair of locations). The correlation coefficients and associated p-values obtained using linear regression indicate that performance was independent of inter-source distance. (B) Same as in (A) but using data from interacting patches (case: intra-patch coh =1) and across 3 coupling strengths, 3 SNR values and 3 patch sizes (i.e. 27 combinations for each of the 600 pairs of locations). Statistically significant effects (negative correlations) were observed when using DICS and LCMV. (C) Same as in (B) but this time with the 50 configurations of coupled patches for which partially coherent time series were generated (case: intra-patch coh =0.2). For this condition, we used 2 patch sizes (0.6 cm^2 and 2 cm^2) and the 3 SNR values (i.e. 6 combinations). Here weaker tendencies were observed in the correlation analyses. Note that, for patches, inter-source distance on the x-axis is calculated as the distance between the centroids of the two patches; yielding minimal distance of 10 cm (if we consider the distance between patch edges, the minimal distance is 7.3 cm).

4. Discussion

The main objective of this study was to compare the effect of using one of three distinct MEG inverse solution methods on source-level cortico-cortical coherence estimation. This was carried out using extensive simulations of pairs of sources with variable sizes, levels of intra and inter-source coherence and noise (SNR) conditions. Our main findings suggest that, for point-like sources (two coupled single-dipole sources), the spatial filters (LCMV and DICS) provided a better estimation of coherence, whereas MNE provided better coherence reconstructions when the simulated sources consisted of extended patches. This was the case irrespective of inter-patch coherence level, as long as the time series inside each individual patch were perfectly coherent (intra-patch coherence of 1). More globally, the inverse method used and the form of the simulated sources clearly have an effect on the power and coherence reconstructions: beamformers (LCMV and DICS) have a similar performance in all cases and, on average, have a better performance than MNE for point-like interacting sources, but not for spatially extended sources, where MNE provided better coherence results.

As far as the effect of noise is concerned, we observed that beamformers are more stable to the different values of SNR and have, on average, a better performance than MNE for power estimation, in accordance with (Küçükaltun-Yildirim et al. 2006). In contrast, for coherence reconstructions of coupled patches, MNE shows higher AUC values that expectedly decrease with decreasing SNR. The three methods are sensitive to SNR in point-like simulations. Furthermore, LCMV and DICS perform actually better when the SNR drops from 0 dB to -20 dB. This effect results from the prominent signal cancellation that can occur for beamformers when there is very little noise in the data.

With respect to the strength of coupling, the three methods are sensitive to this parameter for coherence reconstructions. An increasing strength of coupling leads to a better detection of the coherence between the sources and thus a better performance of the three methods. MNE is stable to the different values of strength of coupling for power reconstructions of point-like sources, while the performance of the beamformers improves with the lowest value of strength of coupling. For power reconstructions of patches, all three methods are stable to the different values of strength of coupling.

High within-patch coherence (e.g. identical time series across the vertices of a single patch) adversely affects the results for beamformer-based coherence reconstructions. However, the performance of the beamformers clearly improved when intra-patch coherence was reduced to avoid total intra-patch coupling (Figure 5). This result demonstrates that the drop in connectivity performance observed with beamformers, when simulating each source as a fully coherent patch (identical time series), is caused by a greater propensity for signal cancellation. The mean MNE coherence reconstruction performance in these modified simulations remained stable (Figure 5).

Our results agree with previous reports which conclude that the beamformers successfully reconstruct distant point-like correlated sources in presence of noise (Van Veen et al. 1997; Gross et al. 2001; Hadjipapas et al. 2005; Sekihara et al. 2005; Küçükaltun-Yildirim et al. 2006; Quraan & Cheyne 2010; Steinsträter et al. 2010; Hui et al. 2010). For totally intra-coherent patches, misallocation and cancellation of the signal due to interference of correlated sources reconstruction was observed in accordance to past reports (Barnes et al. 2004). Nonetheless, our results suggest that on average beamformers perform well for power reconstructions but poorly for coherence reconstructions when the elemental dipole activities inside each patch are fully coherent (perfect intra-patch coherence). This effect disappears if intra-patch coherence is reduced.

The time series of the patches which consisted of totally coherent dipoles lead to some inner cancellation of the reconstructed signal, which adversely affects the coherence reconstructions for coupled cortical patches. For source configurations where the beamforming filtering causes partial inner cancellation of the patch signal, the remaining reconstructed signal was enough to contribute as a true positive and account for a high AUC in the power reconstructions but was too weak for coherence estimates. The filtering cancellation was overturned with the partially intra-coherent patches resulting in an improvement of performance for the coherence reconstructions with beamformers. This effect arises from the extended source configuration since the activity at distinct vertices of a patch can be seen as individual sources. When the activity at these vertices is fully coherent, the violation to the beamformer assumption of non-correlated sources negatively affects beamformer performance. It is also interesting to recall, however, that beamforming

provided better coherence reconstructions when the coupled sources were each simulated as a single dipole (point-like source).

Overall, the fairly similar performances of DICS and LCMV were to be expected, as both methods are based on the same algorithm. However, as the estimations of the data covariance are based on different computations, it is possible that the methods would show more marked differences for other types of data and other types of cortico-cortical interactions. It is noteworthy that, although no significant differences were found between the performance of the LCMV and the DICS, DICS shows a slight tendency to perform better for coherence reconstructions and requires substantially less computational time.

Our evaluation of coherence detection was characterized by how accurately the second source is detected when using the first one as a seed point in a brain-wide coherence analysis. In other words, we do not use the result of a source localization procedure to identify the seed. Although this comes with certain limitations, it also allows us to address the two questions separately. In addition, cortico-cortical coupling is not exclusively performed on sources that show significant activations in the source localization step. A selection of a source or a region of interest (ROI) based on the literature (or on a specific hypothesis) is also used as a preliminary step to seed-based source-space coupling analyses. Our results directly apply to such approaches.

It is also important to mention that, like many other coupling measures, coherence estimation is sensitive to field spread effects in MEG (Schoffelen & Gross 2009). In the current study we manually simulated coherence between pairs of sources with variable phase lags (including true zero-phase lag). This constitutes the *real ground truth* for which we test detectability after the estimation of the sources using different inverse methods. Instead of using arbitrary phase-lagged coherence, one could also specifically simulate interactions only with non-zero-phase lags. This would allow for the assessment of the effect of different source estimators on the performance of a family of interaction measures designed to detect non-zero phase-lagged interactions exclusively (cf. Nolte et al. 2004; Stam et al. 2007; Vinck et al. 2011; Brookes et al. 2012; Hipp et al. 2012; O'Neill et al. 2015; Colclough et al. 2015). Despite being over conservative, such metrics are widely used because they are less prone to false positives caused by source leakage. In the present study, we focused on the estimation of coherence because it's a standard and widely established measure, making it a convenient choice given

that our objective is to focus on comparing the impact of various reconstruction methods on connectivity detection. Furthermore, invasive recordings in animals and humans provide evidence for the physiological relevance of coherence and partly suggest that neuronal interactions may indeed exhibit true zero-phase coupling (e.g. Wang et al. 2012; Roelfsema et al. 1997; Frien et al. 1994; Towle et al. 1999; Adhikari et al. 2010; Buffalo et al. 2011; Fries 2005; Buzsáki & Schomburg 2015). This said, it would of course be useful to investigate if the findings reported here hold for a range of other widely-used connectivity metrics such as imaginary coherence, phase-lag index, orthogonalized amplitude coupling and inter-areal cross-frequency coupling metrics.

The inter-source alpha-band interactions generated here yielded, by construction (see Appendix A), variable phase lags including true zero-phase lags. We thus used coherence to recover these interactions because it is in theory sensitive to zero and non-zero phase lag coupling. As mentioned earlier, this may be seen as a limitation which may minimize the implications on current research in the community. We argue that the general validity of coherence as a tool to detect interactions with arbitrary phase lags (including zero lags, which are biologically plausible) makes it a good general starting point to investigate the effect of inverse solution methods on source connectivity estimation. Future studies will have to investigate the performance obtained using other metrics, in particular measures that ignore zero-phase interactions.

The present manuscript also considered cases where only two coherent sources are active simultaneously and where the sensor-level noise is Gaussian and uncorrelated across sensors. Future studies should address the effects of more complex source configurations (with several simultaneous active sources that are both coherent and non-coherent with each other) and more realistic noise profiles (e.g., correlated noise across sensors).

Standard and modified ROC analyses and the associated AUC metrics have often been used to assess and compare the performance of different inverse methods with regards to EEG/MEG source reconstruction with simulated data (Lin et al. 2004; Küçükaltun-Yildirim et al. 2006; Darvas et al. 2004; Grova et al. 2006; Chowdhury et al. 2013; Mattout et al. 2006). Because of potential limitations related to performance evaluation with AUC/ROC metrics (e.g. in the presence of highly unbalanced data), we performed additional analyses where we compared

the results obtained with the standard ROC approach to the output obtained when using two types of modified ROC/AUC approaches (described in section 2.7). As seen in Table 1, there was no significant difference between the conclusions one would draw either from the standard ROC or the modified versions.

Linear imaging methods used to solve the MEG inverse problem (such as MNE and beamformers) can be derived in a Bayesian statistical framework (Auranen et al. 2005; Baillet & Garnero 1997; Belardinelli et al. 2012; López et al. 2014; Mattout et al. 2006; Trujillo-Barreto et al. 2004; Wipf & Nagarajan 2009) within this framework, the estimate of the neural currents is the maximum a posteriori (MAP) of the posterior distribution of the sources given the data. Under Gaussian assumptions for both the noise and sources processes, the MAP coincides with the expected value of the posterior distribution. What really makes each method unique is the specific choice of the prior distribution for the spatio/temporal distribution of the neural current; thus, the various algorithms differ only in their prior assumptions about the structure of the source covariance matrix. Lopez et al (2014) describe how the Parametrical Empirical Bayes (PEB) could be exploited to implement most of the popular MEG inverse methods within the Bayesian framework in the SPM software package. They describe the different approaches to optimize the prior covariance parameters and how their form is related to different prior assumptions about the distribution of cortical activity. For a given dataset, the most likely priors are those that maximize the model evidence. The fitness of any prior covariance matrix to explain measured data can be quantified in terms of Variational Free Energy (Friston et al. 2007)). There are multiple constraints that can be used as prior source covariance matrix R. The simplest assumption, adopted in MNE solution, is that all dipoles have the same prior variance and no covariance, thus R_MNE is the identity matrix; while, in beamforming, the prior source covariance matrix R_BF is a diagonal matrix whose diagonal elements are the variance of the beamformer output. More structured prior covariance matrices are obtained as the weighted sum of multiple prior components and the hyperparameters have to be optimized to obtain the prior maximizing the evidence of the data. From a PEB viewpoint, both MNE and LCMV use a single empirical prior and only one parameter has to be optimized. Here, we only perform a straight-forward comparison of MNE and beamformers (with regards to cortico-cortical connectivity detection performance), and we do not focus on the optimal choice of the prior source covariance matrix. Future work could address the development and assessment of these methods within the PEB framework

in order to compare the performance of different priors under the same optimization framework. Different prior covariance matrices, such as Multiple Sparse Prior, could be taken into account (Wipf & Nagarajan 2009). Other techniques that have been developed to facilitate methods comparison within a common framework could potentially be used to confirm and extend the results of the current study (e.g. Hauk and Stenroos, 2014).

It is noteworthy that the power detection results reported here across the three source estimation methods did not systematically follow the respective connectivity detection performances. For instance, even when failing to detect coherence between patches with total intra-patch coherence, beamformers still performed well on power estimation. This highlights critical differences in the impact of the source estimation methods depending on the type of measure one is trying to determine. One should thus avoid extrapolating insights from studies focusing on localizing brain activity to studies on brain connectivity.

Taken together, the results of this study suggest that the accuracy of MEG connectivity analysis may be differently affected by the properties of the interacting sources depending on whether minimum-norm estimates or spatial filters are employed for source estimations. While coupling between point-like sources was more reliably determined using spatial filters, interacting pairs of extended patches were better identified using minimum-norm. However, the latter effect was no longer true if the intra-patch coherence (coherence between the time series of the adjacent dipoles that make up a single patch) was sufficiently reduced.

One may ask how these observations can help us choose the appropriate inverse solution to use with a real MEG data where the source properties are by definition not known. If a priori information is available about the likely properties of the interacting sources (e.g. (i) close to point-like sources, (ii) focal and highly synchronized patches, or (iii) large and weakly synchronized), the current findings can be used to choose one method over the other. Of course, such a priori information is difficult to obtain. So rather than establishing that one technique is superior to the other in all cases, our findings help us understand potential discrepancies that may arise from applying both methods to a given data set. They also indicate which parameters are critical and which ones matter less.

Unfortunately, the size of active cortical patches and, in particular, the degree of intra-patch synchrony they will typically portray at various sizes are not very well established. We therefore simulated fully and partially synchronous patches of different sizes in order to evaluate how different types of cortical activity would affect the connectivity performance, as a function of the source reconstruction algorithm. It is conceivable, however, that future invasive electrophysiological investigations may allow for a better characterization of patch size and the degree of within-patch and between-patch synchronization in real brain signals. Combining such insights with the findings reported here, may help us make more informed methodological choices.

Paths for future research could include replicating this study with other measures of coupling such as phase-based measures, and using more complex source configurations. Moreover, although we compared three of the most widely used inverse methods, other equally interesting MEG inverse problems exist and are used in the field. The framework described here can be extended to other methods in future studies.

Methods comparison is an important and challenging task, yet it is often an ungrateful endeavor. The use of simulated data and carefully controlled parameter space provides an important theoretical framework that can help us understand the factors that affect method performance. Yet, at the same time, practical implications of simulation-based comparisons are limited by the extent to which the simulations resemble real-life data. Nevertheless, we hope that our findings will be useful to the MEG community, and in particular to researchers and clinicians that wish to use MEG to evaluate long-range coupling across brain areas.

Conflict of interest

The authors declare that there is no conflict of interests regarding the publication of this paper.

Acknowledgements

ASH was supported in part by a scholarship from Comisión Nacional de Ciencia y Tecnología de Chile (CONICYT), Colfuturo – Colombia, by the French ANR project ANR-DEFIS 09-EMER-002 CoAdapt and support from an NSERC (Canada) Discovery Grant (RGPIN-2015-04854). The research was performed within the framework of the LABEX CORTEX (ANR-11-LABX-

0042) of Université de Lyon, within the program ANR-11-IDEX-0007. We thank the Academy of Finland (personal grant to JK) for financial support. DC acknowledges support by FONDECYT Grant Nº 1130758. This research was also undertaken thanks to funding from the Canada Research Chairs program and a Discovery Grant (RGPIN-2015-04854) awarded by the Natural Sciences and Engineering Research Council of Canada to K.J. The authors are thankful to the computing center of the National Institute for Nuclear Physics and Particle Physics (CC-IN2P3-CNRS, Lyon).

Appendix A: Oscillatory time series generation

The time series y(t) of each oscillatory source was generated using the following procedure:

y(t) = exp(j*2*pi*fr(t))), for t=1,...,ntim

where

ntim is the total number of time points (we used ntim=70000)

fr(t) = sum_{i=1:t} iflaw(i) = cumsum(iflaw)(t)

where

iflaw is the normalized instantaneous frequency defined by:

iflaw= base_freq + trand*randn(1,ntim)

where

base_freq is the base frequency of the oscillators relative to sampling frequency

(we used base_freq=0.02, i.e. 12 Hz/600 Hz)

trand=variation in the instantaneous frequency of the oscillators (we used trand= 0.0015)

y(t) = y(t)*conj(y(1)), t=1,...,ntim

y(t) = real(y(t))

Coherent pairs of signals were generated by repeatedly simulating two time series, using the above procedure, in a loop until the required level of coherence was achieved. A Matlab implementation of the full procedure has been made available on *github* at the following address: https://github.com/ahincap/create-coherent-time-series/tree/master

References

Adhikari, A., Topiwala, M.A. & Gordon, J.A., 2010. Synchronized Activity between the Ventral Hippocampus and the Medial Prefrontal Cortex during Anxiety. *Neuron*, 65(2), pp.257–269.

Attal, Y. & Schwartz, D., 2013. Assessment of subcortical source localization using deep brain activity imaging model with minimum norm operators: a MEG study. *PloS one*, 8(3), p.e59856.

Auranen, T. et al., 2005. Bayesian analysis of the neuromagnetic inverse problem with ℓp-norm priors. *NeuroImage*, 26(3), pp.870–884.

Baillet, S. & Garnero, L., 1997. A Bayesian approach to introducing anatomo-functional priors in the EEG/MEG inverse problem. *IEEE Transactions on Biomedical Engineering*, 44(5), pp.374–385.

Baillet, S., Mosher, J.C. & Leahy, R.M., 2001. Electromagnetic Brain Mapping. *IEEE Signal Processing Magazine*, 18(6), pp.14–30.

Barnes, G.R. et al., 2004. Realistic spatial sampling for MEG beamformer images. *Human brain mapping*, 23(2), pp.120–7.

Barnes, G.R. & Hillebrand, A., 2003. Statistical flattening of MEG beamformer images. *Human brain mapping*, 18(1), pp.1–12.

Belardinelli, P. et al., 2012. Source reconstruction accuracy of MEG and EEG Bayesian inversion approaches. *PloS one*, 7(12), p.e51985.

Brookes, M.J., Woolrich, M.W. & Barnes, G.R., 2012. Measuring functional connectivity in MEG: A multivariate approach insensitive to linear source leakage. *NeuroImage*, 63(2), pp.910–920.

Buffalo, E.A. et al., 2011. Laminar differences in gamma and alpha coherence in the ventral stream. *Proceedings of the National Academy of Sciences*, 108(27), pp.11262–11267.

Buzsáki, G. & Schomburg, E.W., 2015. What does gamma coherence tell us about inter-regional neural communication? *Nature Neuroscience*, 18(4), pp.484–489.

Cabral, J. et al., 2014. Exploring mechanisms of spontaneous functional connectivity in MEG: How delayed network interactions lead to structured amplitude envelopes of band-pass filtered oscillations. *NeuroImage*, 90, pp.423–435.

Chang, W.-T. et al., 2015. Combined MEG and EEG show reliable patterns of electromagnetic brain activity during natural viewing. *NeuroImage*, 114, pp.49–56.

Cheng, C.-H. et al., 2015. Effects of aging on the neuromagnetic mismatch detection to speech sounds. *Biological psychology*, 104, pp.48–55.

Chowdhury, R.A. et al., 2013. MEG source localization of spatially extended generators of epileptic activity: comparing entropic and hierarchical bayesian approaches. *PloS one*, 8(2), p.e55969.

Colclough, G.L. et al., 2015. A symmetric multivariate leakage correction for MEG connectomes. *NeuroImage*, 117, pp.439–48.

Colclough, G.L. et al., 2016. *How reliable are MEG resting-state connectivity metrics?*,

Dalal, S.S. et al., 2009. Simultaneous MEG and intracranial EEG recordings during attentive reading. *NeuroImage*, 45(4), pp.1289–1304.

Dale, A.M. et al., 2000. Dynamic Statistical Parametric Mapping: Combining fMRI and MEG for High-Resolution Imaging of Cortical Activity. *Neuron*, 26(1), pp.55–67.

Dale, A.M. & Sereno, M.I., 1993. Improved Localization of Cortical Activity by Combining EEG and MEG with MRI Cortical Surface Reconstruction. *Journal of Cognitive Neuroscience*, 5(2), pp.162–176.

Darvas, F. et al., 2004. Mapping human brain function with MEG and EEG: Methods and validation. *NeuroImage*, 23(SUPPL. 1), pp.289–299.

David, O. et al., 2002. Estimation of neural dynamics from MEG/EEG cortical current density maps: application to the reconstruction of large-scale cortical synchrony. *IEEE transactions on bio-medical engineering*, 49(9), pp.975–87.

van Diessen, E. et al., 2015. Opportunities and methodological challenges in EEG and MEG resting state functional brain network research. *Clinical Neurophysiology*, 126(8),

pp.1468–1481.
Diwakar, M. et al., 2011. Dual-Core Beamformer for obtaining highly correlated neuronal networks in MEG. *NeuroImage*, 54(1), pp.253–63.
Engel, A.K. et al., 2013. Intrinsic Coupling Modes: Multiscale Interactions in Ongoing Brain Activity. *Neuron*, 80(4), pp.867–886.
Fischl, B., 2012. FreeSurfer. *NeuroImage*, 62(2), pp.774–81.
Foster, M., 1961. An Application of the Wiener-Kolmogorov Smoothing Theory to Matrix Inversion. *Journal of the Society for Industrial and Applied Mathematics*, 9(3), pp.387–392.
Frien, A. et al., 1994. Stimulus-specific fast oscillations at zero phase between visual areas V1 and V2 of awake monkey. *Neuroreport*, 5(17), pp.2273–7.
Fries, P., 2005. A mechanism for cognitive dynamics: neuronal communication through neuronal coherence. *Trends in Cognitive Sciences*, 9(10), pp.474–480.
Friston, K. et al., 2007. Variational free energy and the Laplace approximation. *NeuroImage*, 34(1), pp.220–234.
Friston, K., Moran, R. & Seth, A.K., 2013. Analysing connectivity with Granger causality and dynamic causal modelling. *Current opinion in neurobiology*, 23(2), pp.172–8.
Garcés, P. et al., 2016. Multimodal description of whole brain connectivity: A comparison of resting state MEG, fMRI, and DWI. *Human Brain Mapping*, 37(1), pp.20–34.
Grave de Peralta Menendez, R. et al., 1997. Linear inverse solutions with optimal resolution kernels applied to electromagnetic tomography. *Human brain mapping*, 5(6), pp.454–67.
Gross, J. et al., 2001. Dynamic imaging of coherent sources: Studying neural interactions in the human brain. *Proceedings of the National Academy of Sciences of the United States of America*, 98(2), pp.694–9.
Gross, J. et al., 2013. Good practice for conducting and reporting MEG research. *NeuroImage*, 65, pp.349–63.
Gross, J. et al., 2003. Properties of MEG tomographic maps obtained with spatial filtering. *NeuroImage*, 19(4), pp.1329–1336.
Grova, C. et al., 2006. Evaluation of EEG localization methods using realistic simulations of interictal spikes. *NeuroImage*, 29(3), pp.734–753.
Hadjipapas, A. et al., 2005. Assessing interactions of linear and nonlinear neuronal sources using MEG beamformers: a proof of concept. *Clinical neurophysiology : official journal of the International Federation of Clinical Neurophysiology*, 116(6), pp.1300–13.
Hämäläinen, M. et al., 1993. Magnetoencephalography—theory, instrumentation, and applications to noninvasive studies of the working human brain. *Reviews of Modern Physics*, 65(2), pp.413–497.
Hämäläinen, M. & Ilmoniemi, R., 1984. *Interpreting measured magnetic fields of the brain: estimates of current distributions*,
Hämäläinen, M.S. & Ilmoniemi, R.J., 1994. Interpreting magnetic fields of the brain: minimum norm estimates. *Medical & Biological Engineering & Computing*, 32(1), pp.35–42.
Hansen, P., Morten, K. & Salmelin, R. eds., 2010. *MEG: An Introduction to Methods*, Oxford University Press.
Haufe, S. et al., 2011. Large-scale EEG/MEG source localization with spatial flexibility. *NeuroImage*, 54(2), pp.851–859.
Hauk, O., 2004. Keep it simple: a case for using classical minimum norm estimation in the analysis of EEG and MEG data. *NeuroImage*, 21(4), pp.1612–21.
Hauk, O., Wakeman, D.G. & Henson, R., 2011. Comparison of noise-normalized minimum norm estimates for MEG analysis using multiple resolution metrics. *NeuroImage*, 54(3), pp.1966–1974.
Henson, R.N. et al., 2007. Population-level inferences for distributed MEG source localization under multiple constraints: Application to face-evoked fields. *NeuroImage*, 38(3),

pp.422–438.
Hillebrand, A. & Barnes, G.R., 2005. Beamformer analysis of MEG data. *International review of neurobiology*, 68, pp.149–71.
Hincapié, A.-S. et al., 2016. MEG Connectivity and Power Detections with Minimum Norm Estimates Require Different Regularization Parameters. , 2016, pp.12–18.
Hipp, J.F. et al., 2012. Large-scale cortical correlation structure of spontaneous oscillatory activity. *Nature Neuroscience*, 15(6), pp.884–890.
Hsiao, F.-J. et al., 2015. Increased Intrinsic Connectivity of the Default Mode Network in Temporal Lobe Epilepsy: Evidence from Resting-State MEG Recordings. *PloS one*, 10(6), p.e0128787.
Hui, H.B. et al., 2010. Identifying true cortical interactions in MEG using the nulling beamformer. *NeuroImage*, 49(4), pp.3161–74.
Ikezawa, K. et al., 2011. Decreased α event-related synchronization in the left posterior temporal cortex in schizophrenia: a magnetoencephalography-beamformer study. *Neuroscience research*, 71(3), pp.235–43.
Jerbi, K. et al., 2007. Coherent neural representation of hand speed in humans revealed by MEG imaging. *Proceedings of the National Academy of Sciences*, 104(18), pp.7676–7681.
Kanamori, Y. et al., 2013. Minimum norm estimates in MEG can delineate the onset of interictal epileptic discharges: A comparison with ECoG findings. *NeuroImage. Clinical*, 2, pp.663–9.
Küçükaltun-Yildirim, E., Pantazis, D. & Leahy, R.M., 2006. Task-based comparison of inverse methods in magnetoencephalography. *IEEE transactions on bio-medical engineering*, 53(9), pp.1783–93.
Kujala, J. et al., 2012. Neural interactions at the core of phonological and semantic priming of written words. *Cerebral cortex (New York, N.Y. : 1991)*, 22(10), pp.2305–12.
Kujala, J., Gross, J. & Salmelin, R., 2008. Localization of correlated network activity at the cortical level with MEG. *NeuroImage*, 39(4), pp.1706–20.
Laaksonen, H. et al., 2012. MEG evoked responses and rhythmic activity provide spatiotemporally complementary measures of neural activity in language production. *NeuroImage*, 60(1), pp.29–36.
Liljeström, M. et al., 2005. Neuromagnetic localization of rhythmic activity in the human brain: a comparison of three methods. *NeuroImage*, 25(3), pp.734–45.
Lin, F.-H. et al., 2004. Spectral spatiotemporal imaging of cortical oscillations and interactions in the human brain. *NeuroImage*, 23(2), pp.582–95.
Lin, F.H. et al., 2006. Assessing and improving the spatial accuracy in MEG source localization by depth-weighted minimum-norm estimates. *NeuroImage*, 31(1), pp.160–171.
Litvak, V. et al., 2010. Optimized beamforming for simultaneous MEG and intracranial local field potential recordings in deep brain stimulation patients. *NeuroImage*, 50(4), pp.1578–88.
Liu, A.K. et al., 1998. Spatiotemporal imaging of human brain activity using functional MRI constrained magnetoencephalography data: Monte Carlo simulations. *Proceedings of the National Academy of Sciences of the United States of America*, 95(15), pp.8945–50.
Lopes da Silva, F., 2013. EEG and MEG: Relevance to neuroscience. *Neuron*, 80(5), pp.1112–1128.
López, J.D. et al., 2014. *Algorithmic procedures for Bayesian MEG/EEG source reconstruction in SPM*,
Luo, L. et al., 2010. Ten years of Nature Reviews Neuroscience: insights from the highly cited. *Nature Reviews Neuroscience*, 11(10), pp.718–726.
Matsuura, K. & Okabe, Y., 1995. Selective minimum-norm solution of the biomagnetic inverse problem. *IEEE Transactions on Biomedical Engineering*, 42(6), pp.608–615.

Mattout, J. et al., 2006. MEG source localization under multiple constraints: an extended Bayesian framework. *NeuroImage*, 30(3), pp.753–67.
Mattout, J. et al., 2005. Multivariate source prelocalization (MSP): use of functionally informed basis functions for better conditioning the MEG inverse problem. *NeuroImage*, 26(2), pp.356–73.
Meeren, H.K.M. et al., 2013. Different cortical dynamics in face and body perception: a MEG study. *PloS one*, 8(9), p.e71408.
Mesulam, M.-M., 1990. Large-scale neurocognitive networks and distributed processing for attention, language, and memory. *Annals of Neurology*, 28(5), pp.597–613.
Mišić, B. & Sporns, O., 2016. From regions to connections and networks: new bridges between brain and behavior. *Current Opinion in Neurobiology*, 40, pp.1–7.
Muthuraman, M. et al., 2015. EEG-MEG Integration Enhances the Characterization of Functional and Effective Connectivity in the Resting State Network. *PloS one*, 10(10), p.e0140832.
Nolte, G. et al., 2004. Identifying true brain interaction from EEG data using the imaginary part of coherency. *Clinical Neurophysiology*, 115(10), pp.2292–2307.
Nunez, P.L. & Srinivasan, R., 2006. *Electric Fields of the Brain: The Neurophysics of EEG*, Oxford University Press.
O'Neill, G.C. et al., 2015. Measuring electrophysiological connectivity by power envelope correlation: a technical review on MEG methods. *Physics in Medicine and Biology*, 60(21), pp.R271–R295.
Oostenveld, R. et al., 2011. FieldTrip: Open source software for advanced analysis of MEG, EEG, and invasive electrophysiological data. *Computational Intelligence and Neuroscience*, 2011.
Palva, S., Monto, S. & Palva, J.M., 2010. Graph properties of synchronized cortical networks during visual working memory maintenance. *NeuroImage*, 49(4), pp.3257–68.
de Pasquale, F. et al., 2012. A Cortical Core for Dynamic Integration of Functional Networks in the Resting Human Brain. *Neuron*, 74(4), pp.753–764.
Phillips, C. et al., 2005. An empirical Bayesian solution to the source reconstruction problem in EEG. *NeuroImage*, 24(4), pp.997–1011.
Pittau, F. & Vulliemoz, S., 2015. Functional brain networks in epilepsy. *Current Opinion in Neurology*, 28(4), pp.338–343.
Popescu, M. et al., 2008. Spatio-temporal reconstruction of bilateral auditory steady-state responses using MEG beamformers. *IEEE transactions on bio-medical engineering*, 55(3), pp.1092–102.
Quraan, M.A. et al., 2011. Detection and localization of hippocampal activity using beamformers with MEG: a detailed investigation using simulations and empirical data. *Human brain mapping*, 32(5), pp.812–27.
Quraan, M.A. & Cheyne, D., 2010. Reconstruction of correlated brain activity with adaptive spatial filters in MEG. *NeuroImage*, 49(3), pp.2387–400.
Roelfsema, P.R. et al., 1997. Visuomotor integration is associated with zero time-lag synchronization among cortical areas. *Nature*, 385(6612), pp.157–161.
Rossiter, H.E. et al., 2012. Changes in the location of cortico-muscular coherence following stroke. *NeuroImage. Clinical*, 2, pp.50–5.
Sarvas, J., 1987. Basic mathematical and electromagnetic concepts of the biomagnetic inverse problem. *Physics in medicine and biology*, 32(1), pp.11–22.
Schnitzler, A. & Gross, J., 2005. Normal and pathological oscillatory communication in the brain. *Nature Reviews Neuroscience*, 6(4), pp.285–296.
Schoffelen, J.-M. & Gross, J., 2009. Source connectivity analysis with MEG and EEG. *Human brain mapping*, 30(6), pp.1857–65.

Schölvinck, M.L. et al., 2013. The contribution of electrophysiology to functional connectivity mapping. *NeuroImage*, 80, pp.297–306.
Sekihara, K. et al., 2001. Reconstructing spatio-temporal activities of neural sources using an MEG vector beamformer technique. *IEEE transactions on bio-medical engineering*, 48(7), pp.760–71.
Sekihara, K., Sahani, M. & Nagarajan, S.S., 2005. Localization bias and spatial resolution of adaptive and non-adaptive spatial filters for MEG source reconstruction. *NeuroImage*, 25(4), pp.1056–67.
Simanova, I. et al., 2015. Predicting the semantic category of internally generated words from neuromagnetic recordings. *Journal of cognitive neuroscience*, 27(1), pp.35–45.
Sorrentino, A. & Pascarella, A., 2011. *Magnetoencephalography* E. Pang, ed., InTech.
Spaak, E., de Lange, F.P. & Jensen, O., 2014. Local entrainment of α oscillations by visual stimuli causes cyclic modulation of perception. *The Journal of neuroscience : the official journal of the Society for Neuroscience*, 34(10), pp.3536–44.
Stam, C.J., Nolte, G. & Daffertshofer, A., 2007. Phase lag index: Assessment of functional connectivity from multi channel EEG and MEG with diminished bias from common sources. *Human Brain Mapping*, 28(11), pp.1178–1193. Available at: http://www.ncbi.nlm.nih.gov/pubmed/17266107 [Accessed December 17, 2016].
Steinsträter, O. et al., 2010. Sensitivity of beamformer source analysis to deficiencies in forward modeling. *Human brain mapping*, 31(12), pp.1907–27.
Stenroos, M. & Hauk, O., 2013. Minimum-norm cortical source estimation in layered head models is robust against skull conductivity error. *NeuroImage*, 81, pp.265–72.
Tadel, F. et al., 2011. Brainstorm: A User-Friendly Application for MEG/EEG Analysis. *Computational intelligence and neuroscience*, 2011, p.879716.
Tikhonov, A.N. & Arsenin, V.I., 1977. *Solutions of ill-posed problems*, Winston.
Towle, V.L. et al., 1999. Electrocorticographic coherence patterns. *Journal of clinical neurophysiology : official publication of the American Electroencephalographic Society*, 16(6), pp.528–47.
Trujillo-Barreto, N.J., Aubert-Vázquez, E. & Valdés-Sosa, P.A., 2004. Bayesian model averaging in EEG/MEG imaging. *NeuroImage*, 21(4), pp.1300–1319.
Varela, F. et al., 2001. The brainweb: Phase synchronization and large-scale integration. *Nature Reviews Neuroscience*, 2(4), pp.229–239.
Van Veen, B.D. et al., 1997. Localization of brain electrical activity via linearly constrained minimum variance spatial filtering. *IEEE Transactions on Biomedical Engineering*, 44(9), pp.867–880.
Vinck, M. et al., 2011. An improved index of phase-synchronization for electrophysiological data in the presence of volume-conduction, noise and sample-size bias. *NeuroImage*, 55(4), pp.1548–1565.
Wang, J.-Z., Williamson, S.J. & Kaufman, L., 1993. Magnetic source imaging based on the Minimum-Norm Least-Squares Inverse. *Brain Topography*, 5(4), pp.365–371.
Wang, L. et al., 2012. Electrophysiological low-frequency coherence and cross-frequency coupling contribute to BOLD connectivity. *Neuron*, 76(5), pp.1010–20.
Welch, P., 1967. The use of fast Fourier transform for the estimation of power spectra: A method based on time averaging over short, modified periodograms. *IEEE Transactions on Audio and Electroacoustics*, 15(2), pp.70–73.
Wipf, D. & Nagarajan, S., 2009. A unified Bayesian framework for MEG/EEG source imaging. *NeuroImage*, 44(3), pp.947–966.

Highlights

- The impact of inverse method selection on connectivity analyses in MEG is unknown
- Extensive MEG data simulations of interacting sources were performed
- Coherence and power cortical maps were reconstructed with MNE, LCMV and DICS
- Coupling between point-sources was better detected with beamformers than MNE
- Coupling between extended patches was better detected with MNE than beamformers